

Bose-Einstein condensation in a mm-scale Ioffe-Pritchard trap

Kevin L. Moore,* Thomas P. Purdy, Kater W. Murch, Kenneth R.

Brown, Keshav Dani, Subhadeep Gupta, and Dan M. Stamper-Kurn

Department of Physics, University of California, 366 LeConte Hall #7300, Berkeley, CA 94720

(Dated: September 13, 2018)

We have constructed a mm-scale Ioffe-Pritchard trap capable of providing axial field curvature of 7800 G/cm^2 with only 10.5 Amperes of driving current. Our novel fabrication method involving electromagnetic coils formed of hard anodized aluminum strips is compatible with ultra-high vacuum conditions, as demonstrated by our using the trap to produce Bose-Einstein condensates of 10^6 ^{87}Rb atoms. The strong axial curvature gives access to a number of experimentally interesting configurations such as tightly confining prolate, nearly isotropic, and oblate spheroidal traps, as well as traps with variable tilt angles with respect to the nominal axial direction.

PACS numbers: 03.75.Nt, 32.80.Pj, 05.30.Jp

Magnetic traps have become a staple of ultracold atomic physics. As such, innovations in magnetic trapping techniques have consistently led to new experimental breakthroughs. For example, the invention of the time-orbiting-potential (TOP) trap to stem Majorana losses in spherical quadrupole traps led to the first gaseous Bose-Einstein condensates (BECs) [1]. The cloverleaf trap [2], the QUIC trap [3], and other electro- and permanent magnet configurations allowed for stable confinement of large BECs with DC fields and variable aspect ratios; these capabilities led, for example, to precise tests of mean-field theories [4], observations of quasi-condensates in reduced dimensions [5], and studies of long-lived hyperfine coherences in two-component gases [6]. The rapidly-developing magnetic-trapping technology of atom chips now provides new capabilities for manipulating ultracold atoms and studying their properties (e.g. coherence of condensates in a waveguide [7], the decay of doubly-charged vortices in a BEC [8], etc.).

A typical configuration for magnetic trapping with DC magnetic fields is the Ioffe-Pritchard (IP) trap [9]. Near the trap center — at distances small compared to the size of or distance to the magnets used to generate the trapping fields — an IP trap is characterized by three quantities: the axial bias magnetic field B_0 , the radial quadrupole field gradient B'_ρ , and the axial field curvature B''_z . The magnitudes of these parameters scale as I/d , I/d^2 and I/d^3 , respectively, where I is the total current carried in the wire(s) (or magnetization of ferromagnets), and d is their characteristic length scale or distance from the location of the magnetic trap center. Both because of this scaling, and because the effective radial curvature can be greatly increased by lowering the bias field B_0 , the limitation to the confinement strength of an IP trap comes typically from the maximum axial curvature which can be attained.

As indicated by the I/d^3 scaling of the axial curvature, strategies for increasing the confinement of an IP trap in-

volve both increasing the current in the coils and decreasing the characteristic size scale of the trap. Magnetic traps used in most ultracold atom experiments have been constructed on one of two different length scales. Centimeter (inch) scale traps, which provide superior optical access, utilize currents of 1000's of Amperes, typically distributed as smaller currents in each of several turns of wire. The highest currents sustainable in such traps, limited by resistive heating, restrict axial field curvatures to the neighborhood of 100 G/cm^2 .

Alternatively, magnetic confinement can be provided with modest currents by reducing the field-producing wires and their distance to the ultracold atoms to microscopic sizes. This strategy has been carried out effectively with surface microtraps [10, 11, 12], resulting in versatile ultracold atomic experiments. The typical size scale for these microfabricated magnetic traps is $\sim 100 \mu\text{m}$, and typically only 1 A of current is required to produce IP traps with field curvatures in excess of 10^4 G/cm^2 [11, 13]. Microtraps are not ideally suited for all experimental endeavors, however, as the atomic cloud is trapped $\sim 100 \mu\text{m}$ or less from the planar surface.

In this article we describe the design, construction, operation, and performance of a millimeter-scale, $\sim 10 \text{ A}$ (or ~ 100 Ampere-turns) magnetic trap which bridges the two aforementioned regimes. This “millitrap” utilizes a novel fabrication scheme which allows for the production of axial field curvatures of over 7800 G/cm^2 and is shown to be compatible with experimental requirements for the creation of large BECs. We demonstrate that this trap, owing to its high axial field curvature, allows for a wide range of trapping geometries, ranging from the typical prolate spheroidal to the more unusual oblate spheroidal configuration. Further, we describe a modification of the IP trapping fields which allows for traps with a variable tilt angle with respect to the nominal axial direction, a capability which is compatible with excitation of the “scissors mode” [14], the creation of vortices [15, 16] or other studies of superfluid flow [17, 18] in a BEC. The trap is also suitable for loading and trapping an ultracold atomic gas inside a high-finesse cavity formed by conventional mm-scale mirrors [19, 20, 21] (or near other

*Electronic address: klmoores@socrates.berkeley.edu

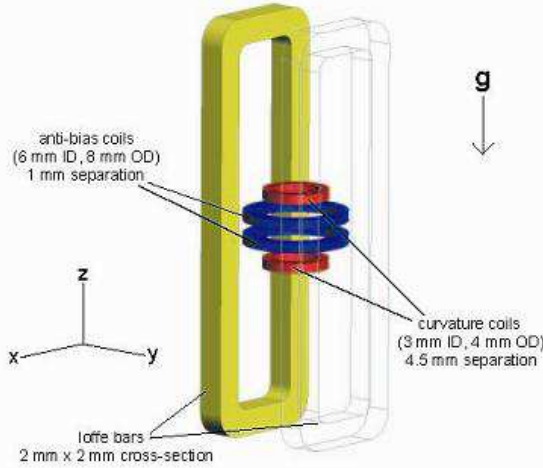


FIG. 1: Sketch of the mm-scale IP trap. The primary curvature coils (red), the anti-bias coils (blue), and the gradient coils (yellow) are depicted in this diagram as solid bodies, but are in actuality multiple turns of wire with protruding leads. For clarity the coil leads have been omitted and the nearest gradient coil is shown as transparent. *Higher resolution version of figures at <http://physics.berkeley.edu/research/ultracold>.*

mm-scale objects).

The winding pattern of the millitrap is similar to that of inch-scale IP traps (see Figs. 1 and 2). The axial field is shaped by two pairs of coaxial coils, with parallel currents in each pair of coils but opposite currents in each of the two pairs. The small diameter coils (“curvature coils”) are positioned to generate the maximum possible curvature given their diameter. The larger diameter coils (“anti-bias coils”) allow for near cancelation of the large bias field produced by the curvature coils at the trap center, while their small axial separation allows for a slight increase (about 15 %) in the total axial curvature. Finally, two elongated rectangular coils (“gradient coils”), run antiparallel currents to produce a radial quadrupole field. The dimensions of various coils were chosen to maximize axial curvature while allowing for a 3 mm diameter cylindrical clearance along the trap axis (for the later accommodation of mirrors for a Fabry–Perot cavity), and a 1 mm clearance along the radial directions for the purpose of imaging. Further details on the positioning and cross sectional area of the coils are shown in Table I.

To maximize the current density while avoiding large input currents and uncontrolled magnetic fields from current leads, multi-turn coils (with total cross sections on the order of 1 mm^2) were used. The maximum current density attainable in coils fabricated by various methods is limited by the steady state temperature of the coils, due to the tendency of the coil resistance to rise with temperature. We found that, for all implementations, there is a threshold at which no more current can be

added to a coil without the resistance increasing exponentially from overheating. Thus, in order to minimize resistive heating and maximize heat dissipation, it is desirable to choose a fabrication method which allows for the cross-sectional area to be efficiently packed with current carrying conductor rather than electrical (and typically thermal) insulation.

Guided by these criteria, we chose to form electromagnetic coils from multiple turns of hard-anodized pure aluminum foil strips. The assembly procedure is illustrated in Fig. 2. Shear-cut strips of aluminum foil were cleaned and then hard anodized in sulfuric acid after smoothing their jagged edges with lubricated fine grit sandpaper. The thickness of the insulating Al_2O_3 layer (on the order of microns) was controlled by varying the duration of the anodization, and chosen to be thick enough to reliably prevent current shorts between turns of the coil but thin enough to allow the coils to be wound without fracture. Coils were then wound on Teflon mandrels with a UHV-compatible, thermally-conductive epoxy applied between turns. The epoxy was set by baking the coil and mandrel at 150°C for two hours, after which the coil was removed and then tested for electrical shorts through both DC resistance measurements and AC magnetic field measurements.

The coils were then inserted into a compound mounting and heat-sinking structure and secured by epoxy (curvature and antibias coils) or by pressure (gradient coils). Portions of the mount in contact with the coils were formed from hard-anodized aluminum. Current connections to the coil were formed by removing oxide layers from the leads and then clamping them tightly between two pieces of copper. Finally, the trap and mounting structure was installed in a UHV vacuum chamber, with current connection made through polyimide-insulated copper wires to a set of 20 A vacuum current feedthroughs. The mounting structure also contains two hollow channels for circulation of liquid nitrogen. Operating the magnetic trap at liquid nitrogen temperatures lowers the resistance of the aluminum coils by a factor of four compared to that at room temperature, allowing higher current densities to be maintained. Following a bakeout of the millitrap at a temperature of 250°C , lifetimes of over 100 s were observed for atoms trapped in the millitrap, demonstrating the vacuum compatibility of all materials used in its construction.

To provide the most flexibility in operating the millitrap, separate electrically-floating power supplies were used for each coil. Also included in the electrical setup were a set of inductor-capacitor filters and an interlock system to protect the millitrap from overheating. Electrical characterization of the millitrap following the vacuum bakeout revealed several undesired low-resistance (several Ohm) connections between different coils, indicating electrical connections through the common mounting structure. These inter-coil connections should have no effect since independent supplies are used for each coil. The possible presence of undesired intra-coil connections,

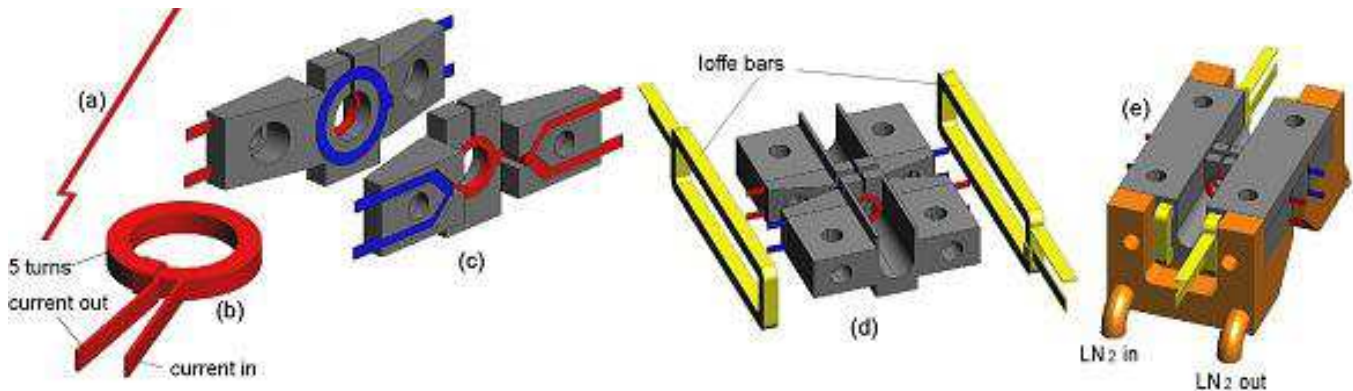


FIG. 2: Sketch of the assembly procedure and part integration. (a) Aluminum strips were cut with a z-shaped pattern to allow for the extraction of the interior current channel after the coil is wound. (b) A curvature coil with input and output current leads. (c) Curvature coils (red) and anti-bias coils (blue) were epoxied into anodized aluminum (grey) faceplates; current leads protrude from sides. (d) The faceplates were attached to an anodized aluminum mount which allows the gradient coils (yellow) to slide over the assembly. (e) A top fixture plate holds the mount in place by bolting into a copper mount (orange) below. A closed path inside the copper piece allows liquid nitrogen to be circulated.

TABLE I: Parameters for aluminum coil windings.

Coil	Inner Diam.	Outer Diam.	Foil thickness	Width	Cross-section	No. turns	Heat generated @ 10 A
curvature	3 mm	4 mm	0.006 in.	1 mm	0.5 mm ²	5	2 Watts
anti-bias	6 mm	8 mm	0.008 in.	0.75 mm	0.75 mm ²	4	2 Watts
gradient	N/A	N/A	0.008 in.	2 mm	4 mm ²	9	10 Watts

e.g. connections between turns on the multiple-turn coils, was tested by measuring parameters of magnetic traps formed with varying currents in each of the curvature, anti-bias, and gradient coils. No clear evidence for such flaws was obtained.

Cold atoms were loaded into the millitrap by optically cooling and trapping atoms in one portion of the UHV chamber, and then magnetically transporting them to the millitrap region. This multi-stage experimental procedure is depicted in Fig. 3. In a “loading region” which is displaced 3 inches horizontally from the millitrap, a 5×10^9 atom MOT was loaded from a Zeeman slowed beam of ^{87}Rb . About 2×10^9 atoms were trapped in the $|F = 1, m_F = -1\rangle$ magnetic sublevel by a spherical quadrupole magnetic trap with an axial gradient of 200 G/cm. The atoms were then transported using two sets of stationary anti-helmholtz coil pairs external to the chamber (similar to Ref. [22]), one of which is centered at the “loading region” and which is used for the initial spherical quadrupole trap and the other centered at the millitrap. As the two anti-helmholtz coil pairs overlap each other, the magnetically-trapped cloud was easily transported between the two coil centers by varying the currents in the two quadrupole coil pairs. During this transport, the atomic cloud was cooled by RF evaporation to reduce the cloud size to about 400 μm before passing the atoms through the 1 mm gap between the millitrap anti-bias coils.

Transfer of the atoms from the external-coil-based

spherical quadrupole trap to the IP trap was accomplished in two stages of “handshaking.” First, atoms were transferred to a spherical quadrupole trap formed by two of the six millitrap coils (a curvature coil and an opposing anti-bias coil); at 2 A running through each of these coils, a quadrupole trap with 150 G/cm axial gradient was produced, nearly matching the field strength generated by 400 A of current running through the external quadrupole coils. The spherical quadrupole trap was then suddenly (within 100 μs) replaced with the IP millitrap. This sudden quadrupole-to-IP transfer caused 25% (or less) of the atoms to be lost. RF evaporative cooling was then performed in a prolate IP trap, with trapping frequencies of $(\omega_x, \omega_y, \omega_z) = 2\pi \times (151, 138, 52)$ Hz (axes oriented as in Fig. 1), yielding atomic clouds near or below the BEC transition temperature (about 300 nK for our system). The transition temperature was reached with 2.5×10^6 atoms, and nearly pure condensates of 1×10^6 atoms produced upon further cooling.

The strongest confinement provided by the millitrap depends on whether such confinement is provided for long or for short trapping times. For example, up to about 7 A of current can be maintained in the curvature and anti-bias coils on a steady-state basis. Coils were safely operated at higher currents, up to about 11 A, although we found that after about 100 ms, the resistive heating of the coils led to increased outgassing which worsened the vacuum conditions in the millitrap region. The axial curvature provided under these conditions was mea-

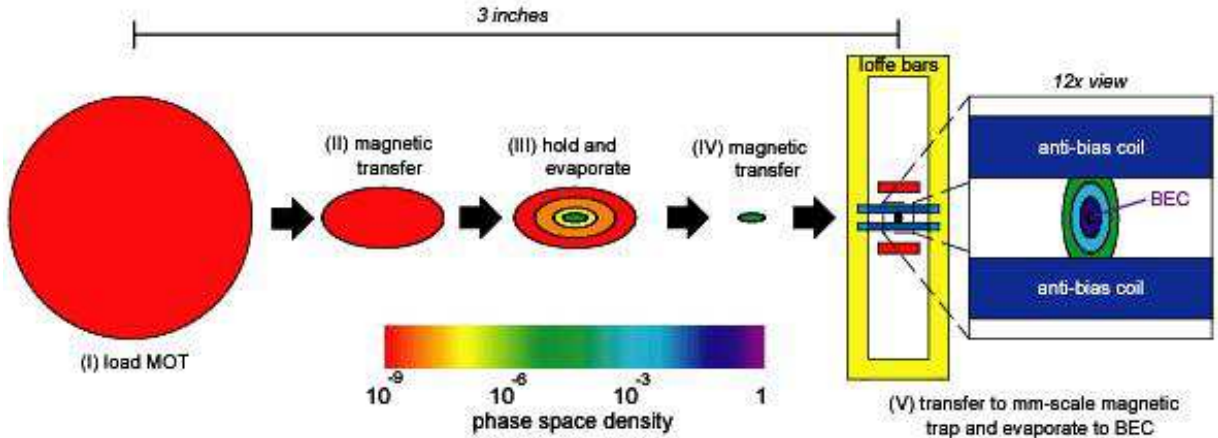


FIG. 3: Sketch of experimental sequence. (I) Atoms are loaded into the MOT and subsequently trapped in a spherical quadrupole trap. (II) The atoms are then transferred 1.75 inches towards the mm-scale IP trap and (III) evaporated to a phase space density of $\Gamma \sim 10^{-5}$. (IV) The cloud is magnetically transferred into the IP trap and (V) captured by a curvature coil and an anti-bias coil in a spherical quadrupole trap. The full millitrapped is then turned on and the atoms are confined in the IP field with a 2 G bias field. The cloud is then further evaporated, forming a pure BEC of 1 million atoms.

sured in-situ using the trapped atoms as a probe, both by measuring the axial oscillation frequency of the trapped cloud, as well as by measuring the axial displacement of the cloud due to the application of a known axial field gradient. From these measurements, we determine that steady-state axial curvatures of 5300 G/cm^2 (7 A setting) and brief confinement with 7800 G/cm^2 (10.5 A setting) can be reached. Gradient coils are operated at a maximum of 11 A, yielding radial gradients of 220 G/cm .

One unexpected feature of this strong IP trap is a remarkably high efficiency of RF evaporation. This efficiency can be quantified by comparing the factor gained in phase space density Γ through the evaporative cooling loss of a given factor in atom number N , obtaining, e.g. a figure of merit $f = -d \ln \Gamma / d \ln N$, with Γ and N parameterized along some evaporation trajectory. Typical figures of merit cited in the literature for evaporation from IP traps are $f = 2$ to $f = 3$ [23, 24]. In our mm-scale IP trap, a factor of over 10^5 in phase space density is efficiently gained by evaporative cooling to the Bose-Einstein condensation transition temperature with an overall figure of merit of $f = 4.5$.

To account for this high efficiency, we note that the IP trap, aside from being strongly confining and thus compressing atomic clouds to high collision rates, is also nearly isotropic. We suspect that the condition of near isotropy improves the efficiency of evaporative cooling relative to that in the typically-used anisotropic traps since high-energy atoms produced collisionally in the gas can easily escape the center of the cloud in *any direction*, and thereby reach the trap boundary established by the applied RF radiation. In contrast, in a cigar-shaped cloud with high aspect ratio, the large axial collisional depth can prevent the escape of all high-energy atoms except those travelling nearly purely in the radial direction. Further, we note that high evaporation efficiency is

obtained in our trap in spite of the vertical orientation of the axial direction; in contrast, IP traps with weaker axial confinement are rarely oriented in this manner so as to avoid the onset of lower dimensional evaporation due to gravitational sag [24, 25].

We have investigated several new features which are afforded by the large axial curvature in our trap. For instance, considering the generic magnetic field configuration of an IP trap and expanding about the minimum of the magnetic field, an effective radial curvature is obtained as $B''_\rho = B'^2_\rho / B_0 - B''_z / 2$. The dependence of the radial trap strength on the applied bias field B_0 offers a simple means of varying the aspect ratio of the trap arbitrarily, ranging from prolate ($B''_z > B''_\rho$) to near-isotropic ($B''_z \simeq B''_\rho$) to oblate ($B''_z < B''_\rho$) geometries. While experiments using IP traps have typically employed prolate or near-isotropic geometries, the oblate geometry has been avoided since the very weak confinement afforded by such traps (limited to below the already weak axial confinement), makes it difficult to compensate for gravitational sag and stray magnetic fields. Thus, by greatly boosting the typical axial confinement strength, our trap gives more convenient access to oblate DC magnetic traps, with advantages for the study of two-dimensional [26, 27, 28] and/or rotating condensates.

Fig. 4 shows the range of trapping geometries accessed by our millitrapped. After evaporatively cooling a thermal gas to a temperature of about 500 nK, the bias field B_0 was ramped to values ranging from 2 G to 18 G while holding the axial curvature at $B''_z \simeq 4000 \text{ G/cm}^2$ and radial gradient at $B'_\rho = 205 \text{ G/cm}$. We then displaced the cloud slightly in this new trap configuration, and recorded the harmonic motion of the trapped cloud to determine trap frequencies along three orthogonal directions. For this purpose, absorption imaging was employed along either of two imaging axes — one through

the 3 mm vertical aperture along the vertical trap axis, and the other along the horizontal \hat{y} direction through the 1 mm gap between the anti-bias coils.

These measurements illustrate the breaking of radial trap symmetry in our trap due to gravity. This can be understood by considering that the atomic cloud sags under gravity to the point where the axial gradient of about 30 G/cm gives a force on atoms in the $|F=1, m_F=-1\rangle$ equal to the gravitational force. By the condition $\vec{\nabla} \cdot \vec{B} = 0$, the presence of this axial gradient implies a radial field gradient of 15 G/cm which breaks the symmetry of the radial quadrupole field, adding to the magnetic field gradient along one direction (\hat{y}) while subtracting from that along the other direction (\hat{x}). Thus, triaxial, rather than cylindrically symmetric, traps are produced.

One motivating factor in our tailoring the aspect ratio of the IP trap is the desire to detect the presence of quantum depletion by precise measurements of collective excitation frequencies, as proposed by Stringari and Pitaevskii [29]. If one considers a fixed condensate number and axial trap strength, one finds that the largest magnitude frequency shift of the lowest collective mode would be obtained with traps that are nearly isotropic; even though higher condensate densities (and hence higher quantum depletion) are produced in prolate traps, the quadrupole modes in this case are more surface-like, rather than compressional, in character, and hence are only weakly affected by depletion effects. In our case, the broken symmetry due to effects of gravity produced, at best, nearly isotropic traps. For instance, Fig. 5 shows time-of-flight absorption images of atoms from a $\omega_x : \omega_y : \omega_z = 0.91 : 1.08 : 1.00$ trap. The familiar pronounced anisotropy of an expanding BEC is absent from such images due to the trap isotropy.

Another feature highlighted by the large axial confinement of our trap is a means to vary the orientation of the trap with respect to the nominal axial direction. This effect arises from considering the effects of displacing the radial quadrupole gradient field so that its zero-field axis no longer coincides with the axis of the curvature fields. That is, one considers the fields

$$\begin{aligned} \vec{B}_{curv} &= B_0 \hat{z} + \frac{B''_z}{2} \left[\left(z^2 - \frac{x^2 + y^2}{2} \right) \hat{z} - z(x\hat{x} + y\hat{y}) \right] \\ \vec{B}_{grad} &= B'_\rho [(x - x_0)\hat{x} - (y - y_0)\hat{y}] \end{aligned} \quad (1)$$

where (x_0, y_0) is the position of the gradient-preferred axis in the $\hat{x} - \hat{y}$ plane. This position is controlled experimentally by applying uniform radial fields to a well-aligned ($x_0 = y_0 = 0$) IP trap. Such misalignment yields both a variable displacement and variable tilt of the resulting magnetic trap, which can be understood as follows. Considering for now just the $z = 0$ plane, the location of the magnetic trap is determined by the competition between \vec{B}_{grad} , which tends to locate the cloud at (x_0, y_0) , and the radial variation of the axial field \vec{B}_{curv} which, for small displacements, exerts a radially repulsive force. The (x, y) position of the resulting field minimum

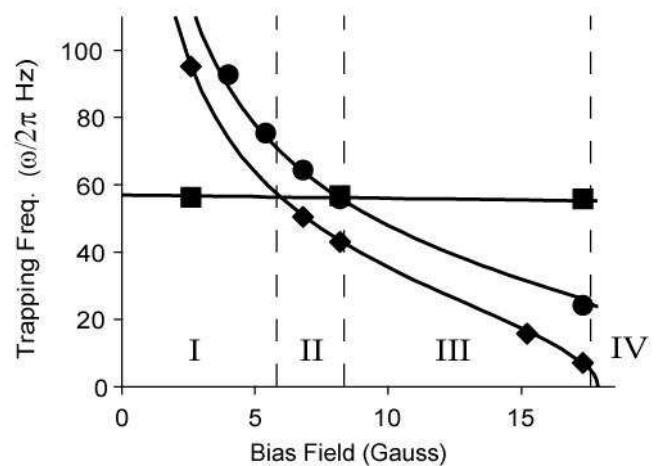


FIG. 4: Measured axial trapping frequency ω_z (squares) and transverse trapping frequencies ω_x (diamonds) and ω_y (circles) as a function of bias field, which was controlled by varying the current in the anti-bias coil pair. The solid lines are theoretical predictions for the trapping frequencies. The only free parameter in the transverse trapping frequency fit is the gradient coil contribution which was allowed to vary within its measured uncertainty. Four distinct regimes can be identified: I - the prolate spheroidal regime (“cigar”-shaped clouds), II - the nearly-isotropic regime, III - the oblate spheroidal regime (“pancake”-shaped), and IV - the unstable regime.

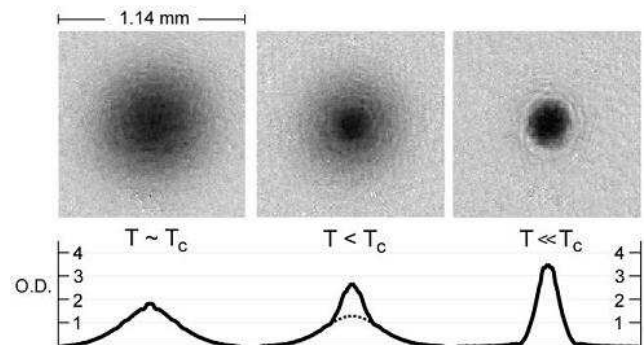


FIG. 5: Absorption images of a nearly-isotropic ultracold gas. Images show separate 36 ms time-of-flight images of a thermal cloud (1.5×10^6 atoms), bimodal distribution, and pure BEC (0.5×10^6 atoms), respectively. The trapping frequencies for this trap are $\{\omega_x, \omega_y, \omega_z\} = 2\pi \times \{52, 62, 57\}$ Hz. Below the images are associated radial averages of the optical densities. The bimodal distribution (center plot) is clearly seen with the condensate rising from the Gaussian fit to the thermal wings (dotted line).

varies for $z \neq 0$ due to the fact that the \vec{B}_{curv} fields now acquire radial components, displacing the position of the radial-field minimum from (x_0, y_0) .

To illustrate this effect, we present in Fig. 6 the tilt angles θ with respect to the \hat{z} axis of the weakest trap axis in a prolate IP trap, as derived from Eqs. 1. Field parameters of $B''_z = 2000$ G/cm², $B'_\rho = 180$ G/cm, and displace-

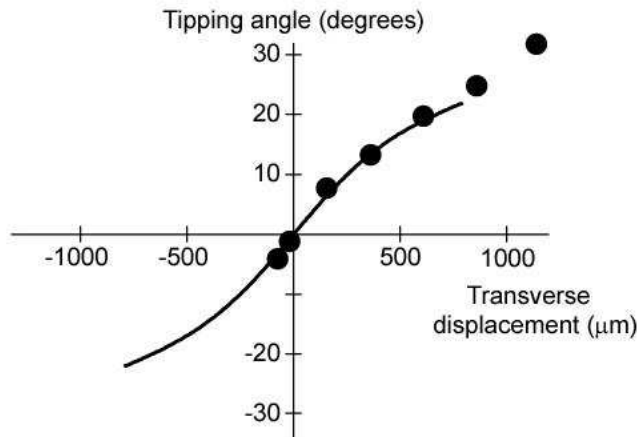


FIG. 6: Tilting atomic clouds in an IP magnetic trap. *In situ* images of tipped prolate clouds yield both the displacement (distinct from x_0) and the tipping angle (data shown as points). These data are compared with calculations (solid line) obtained from the generic IP field expressions of Eqs. 1 for the trap parameters of this experiment ($B_z'' = 2000$ G/cm², $B_p' = 180$ G/cm, and $y_0 = 0$). The theoretical curve is shown only over the range of displacements at which the IP traps (non-zero bias fields) are retained. Beyond this range, the displaced traps become filled, asymmetric spherical quadrupole traps, as presumably applies to the two data at highest displacements.

ments $y_0 = 0$ and variable x_0 are chosen to match experimental settings. The tilt angle varies over a wide range of x_0 , out to a limiting displacement $x_c = 2\sqrt{B_0/B_z''}$ beyond which a non-zero-bias trap is no longer produced.

Aside from varying the tilt angle, this variation of the IP trap also changes the trap frequencies. Indeed, we observed experimentally that the “axial” trap frequency, i.e. the smallest frequency in a prolate IP trap, can be dramatically reduced in the case of a misalignment (x_0 and/or $y_0 \neq 0$). This leads to an apparent discrepancy between this trap frequency, which was determined by following the oscillatory motion of a trapped cloud, and a measurement of B_z'' , as determined from measuring the upward (\hat{z}) displacement of the magnetic trap for a given axial field gradient, when the misalignment was large. Once external fields were applied to correct this

misalignment, the measured trap frequencies and axial field curvatures were in agreement.

In conclusion, we have constructed a novel mm-scale IP magnetic trap which provides the means for tailoring magnetic potentials on length scales intermediate to the larger, inch-scale electromagnets and smaller microfabricated devices. The millimeter length scale is in some ways natural for manipulating cold atomic clouds, generating sufficiently deep and well behaved potentials over the ~ 100 micron scale of typical gaseous samples. This trapping technology may thus provide a flexible means to transport ultracold clouds or construct large scale waveguides appropriate for condensate-based interferometry schemes [7, 30, 31, 32]. Further, making use of the strong axial confinement of the millitrap, we have demonstrated a wide range of trapping geometries which may enable a variety of experiments. For instance, the ability to continuously manipulate the tilt of a cigar-shaped condensate with respect to a fixed axis, simply by the application of uniform magnetic fields, provides a new all-magnetic method for imparting angular momentum to a trapped gas. Compared with laser-based excitation schemes, the utility of which is limited by the length scales of an optical focus (Rayleigh range, beam waist radius) [15], this method may allow the excitation of vortices in BECs with extremely small radial dimensions. Finally, the achievement of large BECs in the millitrap, which by design is compatible with existing technologies for high-finesse Fabry-Perot optical resonators, accomplishes a significant milestone toward the application of cavity quantum electrodynamics to magnetically trapped ultracold atoms.

We acknowledge the skillful work of Dave Murai and Armando Baeza of the UCB Physics Machine Shop in constructing and installing the mount pieces. The authors effort was sponsored by the Defense Advanced Research Projects Agency (DARPA) and Air Force Laboratory, Air Force Materiel Command, USAF, under Contract No. F30602-01-2-0524, the NSF (Grant No. 0130414), the Alfred P. Sloan and David and Lucile Packard Foundations, and the University of California. KLM acknowledges support from the National Science Foundation. SG acknowledges support from the Miller Institute for Basic Research in Science.

-
- [1] M. H. Anderson *et al.*, Science **269**, 198 (1995).
 - [2] M.-O. Mewes *et al.*, Phys. Rev. Lett. **77**, 416 (1996).
 - [3] T. Esslinger, I. Bloch, and T. W. Hänsch, Phys. Rev. A **58**, R2664 (1998).
 - [4] D. M. Stamper-Kurn, H. J. Miesner, S. Inouye, M. R. Andrews, and W. Ketterle, Phys. Rev. Lett. **81**, 500 (1998).
 - [5] S. Dettmer *et al.*, Phys. Rev. Lett. **87**, 160406 (2001).
 - [6] H. J. Lewandowski, D. M. Harber, D. L. Whitaker, and E. A. Cornell, Phys. Rev. Lett. **88**, 070403 (2002).
 - [7] Y.-J. Wang *et al.*, preprint, ArXiv cond-mat/0407689.
 - [8] Y. Shin *et al.*, Phys. Rev. Lett. **93**, 160406 (2004).
 - [9] D. S. Durfee *et al.*, in “Bose-Einstein condensation in atomic gases”, *Proceedings of the International School of Physics, Course CXL*, edited by M. Inguscio, S. Stringari, and C. E. Wieman (IOS Press, Amsterdam, 1999), pp. 67–176.
 - [10] R. Folman *et al.*, Phys. Rev. Lett. **84**, 4749 (2000).
 - [11] W. Hänsel, P. Hommelhoff, T. W. Hänsch, and J. Reichel, Nature **413**, 498 (2001).
 - [12] H. Ott, J. Fortagh, G. Schlotterbeck, A. Grossmann, and

- C. Zimmermann, Phys. Rev. Lett. **87**, 230401 (2001).
- [13] Specialized atom-chip traps have been fabricated which may give axial curvatures up to 10^8 G/cm² [33, 34] .
- [14] O. M. Maragò *et al.*, Phys. Rev. Lett. **84**, 2056 (2000).
- [15] K. W. Madison, F. Chevy, W. Wohlleben, and J. Dalibard, Phys. Rev. Lett. **84**, 806 (2000).
- [16] J. R. Abo-Shaeer, C. Raman, J. M. Vogels, and W. Ketterle, Science **292**, 476 (2001).
- [17] G. Hechenblaikner, E. Hodby, S. A. Hopkins, O. M. Marago, and C. J. Foot, Phys. Rev. Lett. **88**, 070406 (2002).
- [18] S. Stringari, Phys. Rev. Lett. **86**, 4725 (2001).
- [19] C. J. Hood, M. S. Chapman, T. W. Lynn, and H. J. Kimble, Phys. Rev. Lett. **80**, 4157 (1998).
- [20] J. Ye, D. W. Vernooy, and H. J. Kimble, Phys. Rev. Lett. **83**, 4987 (1999).
- [21] P. W. H. Pinsky, T. Fischer, P. Maunz, and G. Rempe, Nature **404**, 365 (2000).
- [22] M. Greiner, I. Bloch, T. W. Hänsch, and T. Esslinger, Phys. Rev. A **63**, 031401(R) (2001).
- [23] J. Arlt *et al.*, J. Phys. B **32**, 5861 (1999).
- [24] W. Ketterle and N. J. van Druten, in *Advances in Atomic, Molecular, and Optical Physics*, edited by B. Bederson and H. Walther (Academic Press, San Diego, 1996), Vol. 37, pp. 181 – 236.
- [25] P. W. H. Pinkse *et al.*, Phys. Rev. A **57**, 4747 (1998).
- [26] A. Gorlitz *et al.*, Phys. Rev. Lett. **87**, 130402 (2001).
- [27] D. Rychtarik, B. Engeser, H.-C. Nägerl, and R. Grimm, Phys. Rev. Lett. **92**, 173003 (2004).
- [28] N. L. Smith *et al.*, arXiv preprint cond-mat/0410101.
- [29] L. Pitaevskii and S. Stringari, Phys. Rev. Lett. **81**, 4541 (1998).
- [30] Y. Shin *et al.*, Phys. Rev. Lett. **92**, 050405 (2004).
- [31] W. Hänsel, J. Reichel, P. Hommelhoff, and T. W. Hänsch, Phys. Rev. A **64**, 063607 (2001).
- [32] E. Andersson *et al.*, Phys. Rev. Lett. **88**, 100401 (2002).
- [33] B. Lev, Nanotechnology **15**, S556 (2004).
- [34] M. Drndić *et al.*, Applied Physics Letters **72**, 2906 (1998).